


# Ginsenoside Rg1 inhibits angiogenesis in diabetic retinopathy through the miR-100-3p/FBXW7/c-MYC molecular axis

Liping Xue<sup>1†</sup>, Min Hu<sup>1†</sup>, Yadi Li<sup>1</sup>, Qin Zhu<sup>1</sup>, Guanglong Zhou<sup>1</sup>, Xiaofan Zhang<sup>1</sup>, Yuan Zhou<sup>1</sup>, Jieying Zhang<sup>1</sup>, Peng Ding<sup>2\*</sup> 

<sup>1</sup>Department of Pediatric Ophthalmology, The Affiliated Hospital of Yunnan University, The Second People's Hospital of Yunnan, The Affiliated Ophthalmology Hospital of Yunnan University, Kunming, China, and <sup>2</sup>Department of Neurosurgery, The First Affiliated Hospital of Kunming Medical University, Kunming, China

## Keywords

Angiogenesis, Diabetic retinopathy, Ginsenoside Rg1

## \*Correspondence

Peng Ding  
Tel.: 13577038792  
Fax: 0871-65323617  
E-mail address:  
[dingp1210@163.com](mailto:dingp1210@163.com)

*J Diabetes Investig* 2025; 16: 791–806

doi: [10.1111/jdi.70016](https://doi.org/10.1111/jdi.70016)

## ABSTRACT

**Aims/Introduction:** Ginsenoside Rg1 is an active ingredient found mainly in ginseng that has a variety of pharmacological effects, such as hypoglycemic, antioxidant, and anti-inflammatory effects, and it inhibits vascular formation. In this study, we explored the effect of ginsenoside Rg1 on angiogenesis in diabetic retinopathy (DR) on the basis of its ability to inhibit angiogenesis and the specific molecular mechanism involved.

**Materials and Methods:** We induced an in vivo model of diabetes by injection of 55 mg/kg streptozotocin (STZ) into the abdominal cavity of SD rats daily for 3 days. Moreover, human retinal microvascular endothelial cells (HRMECs) were treated with 30 mmol/L glucose for 24 h to construct a high-glucose (HG) cell model in vitro. The expression of related genes and proteins was detected by RT-qPCR and Western blotting. HRMECs and retinal damage were evaluated by CCK-8, scratch, tube formation assays, and HE staining.

**Results:** In this study, Rg1 inhibited HG-induced angiogenesis of HRMECs and inhibited STZ-induced vascular leakage and capillary degeneration in vivo, alleviating the progression of DR. Mechanistically, Rg1 upregulated the expression of FBXW7 by inhibiting miR-100-3p, thereby promoting the ubiquitination and degradation of c-MYC, inhibiting HG-induced HRMECs proliferation, migration, invasion, and angiogenesis, and improving the development of DR.

**Conclusions:** Overall, our study demonstrates that ginsenoside Rg1 can inhibit DR angiogenesis via the miR-100-3p/FBXW7/c-MYC molecular axis. These findings provide a novel idea for the treatment of DR and provide an experimental basis for further research on the application of Rg1 in the treatment of DR.

## INTRODUCTION

Diabetic retinopathy (DR), a prevalent microvascular complication of diabetes, is a primary contributor to vision impairment among elderly individuals<sup>1</sup>. By 2010, more than 100 million individuals were impacted by this issue globally, a number projected to surpass 190 million by 2030<sup>2</sup>. The initial clinical manifestations of DR include microaneurysms, hemorrhagic spots, cotton-wool spots, and abnormalities in the microvasculature within the retina<sup>3</sup>. As the severity of DR worsens, capillary

nonperfusion results in retinal ischemia. This ischemia stimulates the overexpression of proangiogenic cytokines, leading to the development of abnormal neovascularization within the retina and vitreous<sup>4</sup>. Laser therapy and vitrectomy, two common treatments for DR, can slow the progression of the disease. However, the use of these therapies in clinical practice is inevitably restricted by specific factors<sup>5</sup>. Consequently, understanding the mechanisms that control DR neovasculation and discovering effective therapeutic drugs are crucial.

For centuries, traditional Chinese medicine has incorporated ginseng into various treatments. A purified saponin known as

†Contributed equally to this work.

Received 8 November 2024; revised 10 February 2025; accepted 18 February 2025

Rg1, derived from ginseng, has shown promising effects, including quick alleviation of tiredness, slowing down the effects of aging, boosting the activity of the central nervous system, preventing blood platelets from sticking together, and improving cognitive functions such as learning and memory<sup>6</sup>. Rg1 has also been shown to be useful for treating obesity<sup>7</sup>, cancer<sup>8</sup>, acute lung injury<sup>9</sup>, and arthritis<sup>10</sup>. In addition, previous studies have shown that Rg1 has strong antioxidant and hypoglycemic activities<sup>11,12</sup>. Our previous studies found that Rg1 inhibited high glucose-induced retinal endothelial cell proliferation, migration, angiogenesis, and VEGF expression through the lncRNA SNG7/mir-216-5p/SIRT3 axis<sup>13</sup>. DR is a complex multifactorial disease whose pathogenesis involves aberrant regulation of numerous molecular pathways and cellular processes. Although the effect of Rg1 on retinal endothelial cells by modulating the lncRNA SNG7/miR-2116-5p/SIRT3 axis has been previously identified, a single molecular axis may not fully explain the full mechanism of action of Rg1 in DR. Therefore, this study will continue to study new molecular axes in order to better understand the role of Rg1 in the development of DR and reveal more potential pathophysiological mechanisms.

MicroRNAs (miRNAs) are a class of single-stranded RNA molecules approximately 20–24 nt long that can specifically inhibit or target specific mRNAs and participate in the regulation of important cell signaling pathways, such as those related to cell development, proliferation, differentiation, and apoptosis<sup>14</sup>. In recent years, many miRNAs have been shown to play a role in regulating the progression of DR<sup>15</sup>. miR-100-3p is a member of a large miRNA family, and the upregulation of miR-100-3p may lead to obesity and insulin resistance, which in turn affect the normal metabolic function of the body<sup>16</sup>. Furthermore, miR-100-3p plays a role in controlling the growth, movement, blood vessel formation, and lymphatic vessel formation of lymphatic endothelial cells<sup>17</sup>. However, the role of miR-100-3p in the progression of DR remains unclear.

Moreover, previous studies in the field of DR have indicated that suppressing F-box and WD-40 domain proteins (FBXW7) can promote angiogenesis in human retinal endothelial cells<sup>18</sup>. FBXW7 is one of the key recognizers of the ubiquitin–proteasome degradation pathway and can reduce the expression of many oncogene proteins, such as c-MYC<sup>19</sup>. More importantly, c-MYC also promotes endothelial cell angiogenesis<sup>20</sup>. Zhang *et al.*<sup>21</sup> reported that eliminating c-MYC may accelerate the secretion of pro-inflammatory cytokines derived from Müller cells, leading to a reduction in the progression of DR in live animals. Therefore, we hypothesized that the FBXW7/c-MYC axis is involved in angiogenesis in DR.

In summary, this study aimed to explore the specific mechanism by which ginsenoside Rg1 inhibits the progression of DR in order to better understand the etiology of DR and provide new ideas and methods for the treatment of DR.

## MATERIALS AND METHODS

### Construction and grouping of animal models

Forty 8-week-old male SD rats weighing between 200 and 240 g were obtained from the Animal Experiment Center at Kunming Medical University. SPF rats are housed at a temperature of 26–28°C, 40–70% humidity, and are provided with a 12 h light and 12 h dark cycle. Following a 1-week acclimatization period, the rats were randomly allocated into four distinct groups. The DR rat model ( $n = 10$ ) was constructed by intraperitoneal injection of streptozotocin (STZ, 55 mg/kg, dissolved in sodium citrate solution, 0.1 mmol/L, pH 4.5) daily for 3 days<sup>22</sup>. Following 3 days, fasting blood glucose was measured by posterior caudal vein sampling. To collect the blood, the rats were gently restrained, and the area around the posterior caudal vein was cleaned and disinfected. A small incision was made, and blood was drawn using a heparin-coated capillary tube. The volume of blood collected was sufficient for measuring fasting blood glucose levels. If the blood glucose concentration was greater than 16.7 mmol/L, the diabetes model was considered to be successfully established. The normal control group ( $n = 10$ ) was given the same dose of sodium citrate buffer as the model group for 3 days. In addition, the Rg1 (HY-N0045, MedChem Express, USA; solvent 10% DMSO and 90% (20% SBE- $\beta$ -CD in saline) were added sequentially to dissolve Rg1) treatment group ( $n = 20$ ) was given 30 or 60 mg/kg Rg1 via intragastric administration to DR rats once a day for 8 weeks. After 8 weeks, body weight and fasting blood glucose levels were measured, and the animals were sacrificed. Rat eyeballs were collected, and five rat eyeballs per group were used for the Evans Blue experiment; the remaining five rat eyeballs in each group were used for the HE staining, immunofluorescence staining, and retinal trypsin digestion experiment.

### Evans blue staining

The rats were anesthetized with 4% isoflurane, cannulated in the right carotid artery and iliac artery, injected with heparin saline, and injected with 45 mg/kg Evans blue in the jugular vein for more than 10 s. After 120 min, the animals were anesthetized, and 0.2 mL of blood was obtained. Subsequently, they were flushed with PBS, and the left ventricle was perfused with 1% paraformaldehyde. The cornea, lens, and vitreous humor were excised, whereas the retina and sclera were fixed in 4% paraformaldehyde at room temperature for 3 min. The treated retinas were immersed in dimethylamide (Sigma Aldrich, St. Louis, MO) at 78°C for a period of 12 h and then subjected to centrifugation at  $12,000 \times g$  for 15 min, followed by exposure to light at 620 nm (blue), and the analysis was performed at 740 nanometers for background measurement.

### Assessment of acellular capillaries

The eyeballs of the rats in both the model and control groups were surgically removed and then preserved in a 4% paraformaldehyde solution for a 24-h period. The retina was

subsequently extracted and treated with 2% trypsin at 37°C for 3 h. The tissue was gently agitated until the retina separated, rinsed thoroughly, mounted onto a glass slide, dried, and subsequently dissociated using a combination of iodate Schiff and hematoxylin staining techniques to visualize the retinal structure.

### HE staining

We collected the eyeballs of the rats and rinsed them with a 1% PBS solution to ensure retinal tissue integrity. Then, the tissue was fixed with 4% paraformaldehyde for 2 h for subsequent experiments. The preserved retinal tissue was then embedded in paraffin and sectioned into thin 5 µm slices. The paraffin-embedded slices were dewaxed in xylene, followed by treatment with a gradient alcohol series, hematoxylin staining for 7 min, differentiation in 5% ethanol for 5 s, and eosin staining for 1 min. Upon completion of staining, a second round of staining with gradient alcohol was conducted. The sections were subsequently allowed to air dry naturally, and the pathological alterations in the retinas of DR rats were observed under a microscope (400857, Nikon, Japan).

### Immunofluorescence

Rat eyeballs were collected and fixed in 4% paraformaldehyde for 2 h. The fixed eyeball was rinsed with PBS, then dehydrated, embedded, and cut into 5 µm slices. The processed sections were incubated at 3 g/L Triton X-100 for 1 h at 4°C. After removal from Triton X-100, goat serum was added dropwise to block antigen at room temperature for 2 h. Aspirate the blocking solution, add appropriate dilutions of CD31 antibody and VEGF antibody dropwise, respectively, place the sections in a wet box, and incubate overnight at 4°C. After the primary antibody incubation, take the sections out of the humid box, rinse with PBS, add the fluorescent-labeled secondary antibody, and incubate in the humid box at room temperature in the dark for 1 h. After the secondary antibody incubation, rinse with PBS, add DAPI staining solution on the sections, and incubate at room temperature in the dark for 10 min. After rinsing with PBS, add anti-fluorescence quenching mounting medium on the sections and cover with a coverslip. Place the mounted slide under a fluorescence microscope (400857, Nikon, Tokyo, Japan) for observation and take pictures for recording.

### Cell culture and transfection

Human retinal microvascular endothelial cells (HRMECs) were acquired from Shenzhen Otwo Biotech Co., Ltd (Item No.: HTX1981). Under the microscope, HRMEC cells were observed to be flat, polygonal, or irregular in shape, and the cells were closely packed and connected to each other to form a paver-like appearance. HRMECs were maintained in DMEM containing 10% fetal bovine serum, 100 U/mL penicillin, and 100 µg/mL streptomycin (Gibco). The cells were incubated at 37°C with 5% CO<sub>2</sub> for standard culture. In vitro culture of the

HRMECs was performed with glucose concentrations of 5.5 and 30 mmol/L for 24 h to establish the normal and high-glucose groups (HG group), respectively<sup>23</sup>. After the HG model was constructed, cells were cultured with 10 mM Rg1 for 24 h. To prepare Rg1 for cell processing, accurately weigh 1 mg of Rg1 powder and dissolve it in cell culture grade DMSO (0.1248 mL) to achieve a final concentration of 10 mM. For the purpose of inhibiting protein synthesis or degradation, 100 µg/mL CHX (a protein synthesis inhibitor) for durations of 0, 1, 3, or 6 h or 20 µM MG132 (protease somatic inhibitor) for 8 h was administered to the cells, after which the c-MYC expression level was assessed via western blot analysis.

HRMECs were cultured overnight in 24-well plates, and when the cell density reached approximately 60–70%, siRNA plasmids or mimics (si-NC, si-FBXW7, NC mimic, or miR-100-3p mimic) were added to the medium at a final concentration of 100 nM according to the instructions of the Lipofectamine 3000 reagent (Invitrogen, Grand Island, NY, USA). The cells were incubated at 37°C in a 5% CO<sub>2</sub> incubator for 48 h, after which the transfection efficiency was measured.

### Western blot analysis

Cell protein extraction: HRMECs in the logarithmic growth phase were digested with pancreatic enzymes, collected in a centrifuge tube, and centrifuged. The supernatant was removed, and RIPA lysis buffer (containing 1% protease inhibitors) was added for cell lysis. Finally, the cell proteins were obtained by centrifuging the lysate and removing the supernatant. Retinal protein extraction: Retinal tissue was removed from the rats, cleaned with precooled saline, cut into small pieces, and added to RIPA lysis buffer. Then, the samples were centrifuged, the supernatant was collected, and tissue protein was obtained. The protein concentrations of the cells and tissues were determined with a BCA detection kit (Thermo Scientific, USA). Total proteins (40 µg per lane) were separated via SDS-PAGE, transferred to PVDF membranes (Millipore, USA), and then blocked with 5% skim milk powder at room temperature for 1.5 h. The membranes were incubated with primary antibodies against FBXW7 (1:1,000, ab192328, Abcam, UK), c-MYC (1:1,000, ab32072, Abcam, UK), and GAPDH (1:1,000, ab181602, Abcam, UK) at 4°C overnight. The membrane was then incubated with a secondary antibody (1:4,000, ab97051, Abcam, UK) at room temperature for 1 h, followed by development with an enhanced chemiluminescence (ECL) kit (Millipore, USA). Finally, semiquantitative analysis of the bands was conducted using ImageJ software (V1.8.0.112, National Institutes of Health, Bethesda, MD, USA).

### RT-qPCR

HRMECs were collected by centrifugation, rat retinal tissue was ground into a fine powder with liquid nitrogen and collected into a centrifuge tube, TRIzol® reagent was added to the centrifuge tube containing cell samples and tissue samples, the cell membrane and organelles were lysed, and RNA was released.

**Table 1** | Primer sequences for RT-qPCR

Target	Sequence (F:Forward primer; R:Reversed primer)
miR-488-5p (HUM)	F:5'-GCGCCCAGATAATGGCAC-3' R:5'-AGTGCAGGGTCCGAGGTATT-3'
miR-577 (HUM)	F:5'-CGCGCGTAGATAAAATATTGG-3' R:5'-AGTGCAGGGTCCGAGGTATT-3'
miR-100-3p (HUM)	F:5'-GCGCGCAAGCTTGTATCTATA-3' R:5'-AGTGCAGGGTCCGAGGTATT-3'
miR-100-3p (RAT)	F:5'-GCGCGCAAGCTTGTGTCT-3' R:5'-AGTGCAGGGTCCGAGGTATT-3'
U6	F:5'-CTCGCTTCGGCAGCACA-3' R:5'-AACGCTTCACGAATTTGCGT-3'

Purified RNA was then obtained by chloroform extraction, isopropanol precipitation, and 75% ethanol washing following the instructions for TRIzol reagent. The RNA was subsequently reverse transcribed into cDNA via a First-Strand cDNA Synthesis Kit (Gennode, China). Real-time fluorescence quantitative PCR was performed using the SYBR Green real-time PCR kit (Solarbio, China), with U6 as an internal reference, and the data were analyzed using the  $2^{-\Delta\Delta C_t}$  method. The sequences of primers used are detailed in Table 1.

### CCK-8

HRMECs were plated at a density of  $5 \times 10^3$  cells per well in 96-well plates and incubated at 37°C in a 5% CO<sub>2</sub> environment for 24 h. The cells were subjected to specific treatments based on their assigned groups. Following treatment, 10 µL of CCK-8 reagent (C0037, Beyotime, China) was added to each well. The optical density at 450 nm was subsequently determined using a microplate reader (ELX800, BioTeK, UK) to assess cell viability.

### Scratch assay

HRMECs that were in the logarithmic growth phase were chosen. Following the standard procedure for digestion and passaging of the cells, they were then plated onto 24-well dishes. Once the cell density reached 90%, a scratch was created using a pipette tip. After 24 h of culture, the migration of the cells was examined using a microscope (Eclipse 80i, Nikon, Tokyo, Japan), and images were captured.

### Transwell assay

Cell invasion was evaluated using Transwell migration invasion nested membranes (LOT 06222041, Corning Incorporated, Corning, NY, USA). The HRMECs in each category were adjusted to a concentration of  $1 \times 10^5$  cells/mL in serum-free DMEM. Two hundred microliters of the cell suspension were placed in the top chamber of a Matrigel-coated Transwell. In the lower chamber of a 24-well plate, 600 µL of DMEM supplemented with 10% fetal calf serum was added. Following a 24-h incubation period, the cells in the lower chamber were

fixed with 4% paraformaldehyde, stained with crystal violet (Solarbio, China), and observed under an inverted microscope (CKX53, OLYMPUS, Japan). The cells were counted at a consistent location within each well, with five fields chosen for counting and visualization.

### Tube formation assay

First, 50 µL of Matrigel was added to a prechilled 96-well plate, and the plate was subsequently placed in an incubator at 37°C for half an hour to allow the Matrigel to solidify into a gel. Following the dissociation of HRMECs from each condition with trypsin, the plates were seeded at a rate of  $2 \times 10^4$ /well. The cells were plated in 96-well plates covered with Matrigel. After the cells were incubated at 37°C in a 5% CO<sub>2</sub> incubator for 12 h, they were examined and imaged using an inverted microscope.

### Ubiquitination assay

MG132 (Sigma-Aldrich), a cell-permeable proteasome inhibitor, was introduced to the cell cultures for a duration of 6 h. Subsequently, immunoprecipitation lysis buffer that included protease inhibitors and phosphatase inhibitors was applied for a period of 30 min. Subsequently, the lysates were subjected to immunoprecipitation using an anti-c-MYC antibody (ab32072, Abcam, UK) at a dilution of 1:500 or immunoglobulin G (IgG; ab6709, Abcam, UK) at a dilution of 1:5,000, and rotation was maintained at 4°C throughout the night. Analysis of c-MYC ubiquitination was performed with an anti-ubiquitin antibody, and the immunoprecipitated proteins were subjected to Western blot analysis.

### Dual-luciferase assay

The predicted binding sites for miR-100-3p and FBXW7 were identified using the bioinformatics website at [https://www.targetscan.org/vert\\_80/](https://www.targetscan.org/vert_80/). The 3'-untranslated region (3'-UTR) of FBXW7, which contains the binding site for miR-100-3p, was subsequently cloned and inserted into the pGL3 vector (Promega) to create the wild-type (WT) FBXW7 vector. Mutations in the FBXW7 vector (MUT) were introduced via a site-directed mutagenesis kit. The 293T cells were cotransfected with either the WT or MUT vectors along with cells overexpressing miR-100-3p or a negative control using Lipofectamine 3000. After a 48-h period, luciferase activity was measured via a dual-luciferase reporter assay system.

### Bioinformatics analysis

The GEOquery package of R software was used to download the MicroRNAs data set GSE74296 from the GEO database. The samples in the data set were *Homo sapiens*, and the samples were based on the GPL21059 platform. Three groups were used as the control group: GSM1917600\_0 mM glucose for 12 h, GSM1917601\_0 mM glucose for 24 h, and GSM1917602\_0 mM glucose for 48 h. Three groups of samples, GSM1917621\_40 mM glucose-24 h and



GSM1917622\_40 mM glucose-48 h, were analyzed as the experimental groups. The differentially expressed genes (DEGs) in the GSE140797 data set were screened via the limma package to determine the differences in the sample DEGs. The ggplot2 package was used to draw volcano maps and heatmaps of the DEGs to visualize the different conditions of the DEGs.

### Statistical analysis

The mean  $\pm$  standard deviation (SD) was used to express all experimental data. GraphPad Prism 7 was used for data analysis and visualization. The cell experiments were repeated at least three times, and the animal experiments were repeated at least five times. Two-group comparisons were conducted via a *t* test, whereas multiple-group comparisons were performed using one-way ANOVA or two-way ANOVA. A statistically significant difference was determined by a *P* value of  $<0.05$ .

## RESULTS

### Ginsenoside Rg1 attenuates diabetes-induced retinal angiogenesis in vivo

First, the impact of Rg1 on DR rats was observed. The body weights and blood glucose levels of the rodents were measured, revealing that STZ administration resulted in a reduction in body weight and an increase in blood glucose levels in the rats. However, these effects were partially mitigated following Rg1 intervention (Figure 1a,b). At the same time, Rg1 treatment can increase insulin levels and glucose transporter GLUT4 expression and inhibit glucose transporter GLUT1 expression (Figure 1c,d). The Evans blue results showed that STZ treatment caused retinal blood vessel dilation, leakage, and leakage spots compared with the Control group, and the Rg1 treatment reduced retinal blood vessel leakage (Figure 1e). Experiments involving trypsin digestion of the retina revealed that retinal blood vessels were disrupted by STZ treatment, exhibited irregular patterns, and had obstructed lumens.<sup>#</sup>*P* < 0.05 Treatment with Rg1 alleviated the deterioration of retinal capillaries following STZ treatment (Figure 1f). HE staining revealed that the arrangement of the retinal inner core layer (INL) and outer nuclear layer (ONL) cells was disordered, the number of ganglion cell layer (GCL) cells was reduced, and the nuclear morphology was abnormal in the STZ group. Rg1 treatment alleviated the pathological changes in retinal tissue (Figure 1g). The immunofluorescence analysis indicated that the administration of STZ resulted in a notable increase in the levels of CD31 and VEGF within the retinal tissues of the rats. Moreover, the impact of these changes was somewhat mitigated following the application of Rg1 (Figure 1h). These results indicate that Rg1 can significantly improve diabetes-induced retinal angiogenesis in rats.

### Ginsenoside Rg1 inhibits high glucose-induced proliferation, migration, invasion, and angiogenesis in HRMECs

Next, the effect of Rg1 on HG-induced HRMECs was examined. First, we observed that the viability of HRMECs was

increased by HG treatment, with the introduction of Rg1 mitigating the HG-triggered increase in cell viability (Figure 2a). In addition, the migration and invasion of HRMECs were induced by HG, whereas treatment with Rg1 resulted in a reduction in both cell migration and invasion (Figure 2b,c). Furthermore, treatment with HG stimulated angiogenesis in HRMECs, whereas the introduction of Rg1 hindered this process (Figure 2d). These findings suggest that Rg1 has the potential to suppress the proliferation, migration, invasion, and angiogenesis triggered by HG in HRMECs.

### Ginsenoside Rg1 inhibition of HRMECs cell proliferation, migration, invasion, and angiogenesis is associated with FBXW7

Previous studies have indicated that the control of FBXW7 expression has the potential to impede neovascularization in diabetic retinopathy<sup>24</sup>. To determine whether Rg1 inhibits HG-induced damage to HRMECs by controlling FBXW7, we first examined FBXW7 expression in HRMECs and rats. Our results revealed that FBXW7 levels were decreased in rats with STZ-induced diabetes and HRMECs exposed to HG, and that treatment with Rg1 increased FBXW7 expression (Figures S1A and 3a). Subsequently, FBXW7 was knocked down in HRMECs, which led to a substantial decrease in FBXW7 expression levels (Figure 3b). Furthermore, knocking down FBXW7 reversed the inhibitory effects of Rg1 on the proliferation, migration, invasion, and angiogenesis of HRMECs induced by HG (Figure 3c–f). These findings demonstrate that ginsenoside Rg1 effectively suppressed the proliferation, migration, invasion, and angiogenesis of HRMECs induced by HG by upregulating FBXW7 expression.

### Ginsenoside Rg1-mediated activation of FBXW7 decreases the protein stability of c-MYC

Previous studies have shown that increased c-MYC levels can increase angiogenesis triggered by HG and facilitate the migration of retinal endothelial cells<sup>25</sup>. Additionally, FBXW7 functions as a recognized c-MYC E3 ubiquitin ligase. Therefore, we explored the subsequent regulatory pathways of FBXW7 to determine whether Rg1 impacts the durability of the c-MYC protein via FBXW7 activation. First, c-MYC levels were assessed in both rats and HRMECs. The results revealed increased c-MYC levels in STZ-induced rats and HG-induced HRMECs. Subsequent Rg1 administration decreased c-MYC levels, whereas FBXW7 knockdown increased c-MYC expression (Figures S1A and 4a). The Western blot results revealed that treatment with Rg1 markedly increased the level of FBXW7 expression and suppressed the expression of c-MYC (Figure 4b). In addition, MG132 was utilized to inhibit protein degradation via proteasomes, followed by analysis of c-MYC expression. The results revealed that in cells treated with Rg1, the degradation level of c-MYC markedly decreased after MG132 treatment. These findings suggest that c-MYC is a substrate for proteasomes (Figure 4c). Next, CHX was applied to

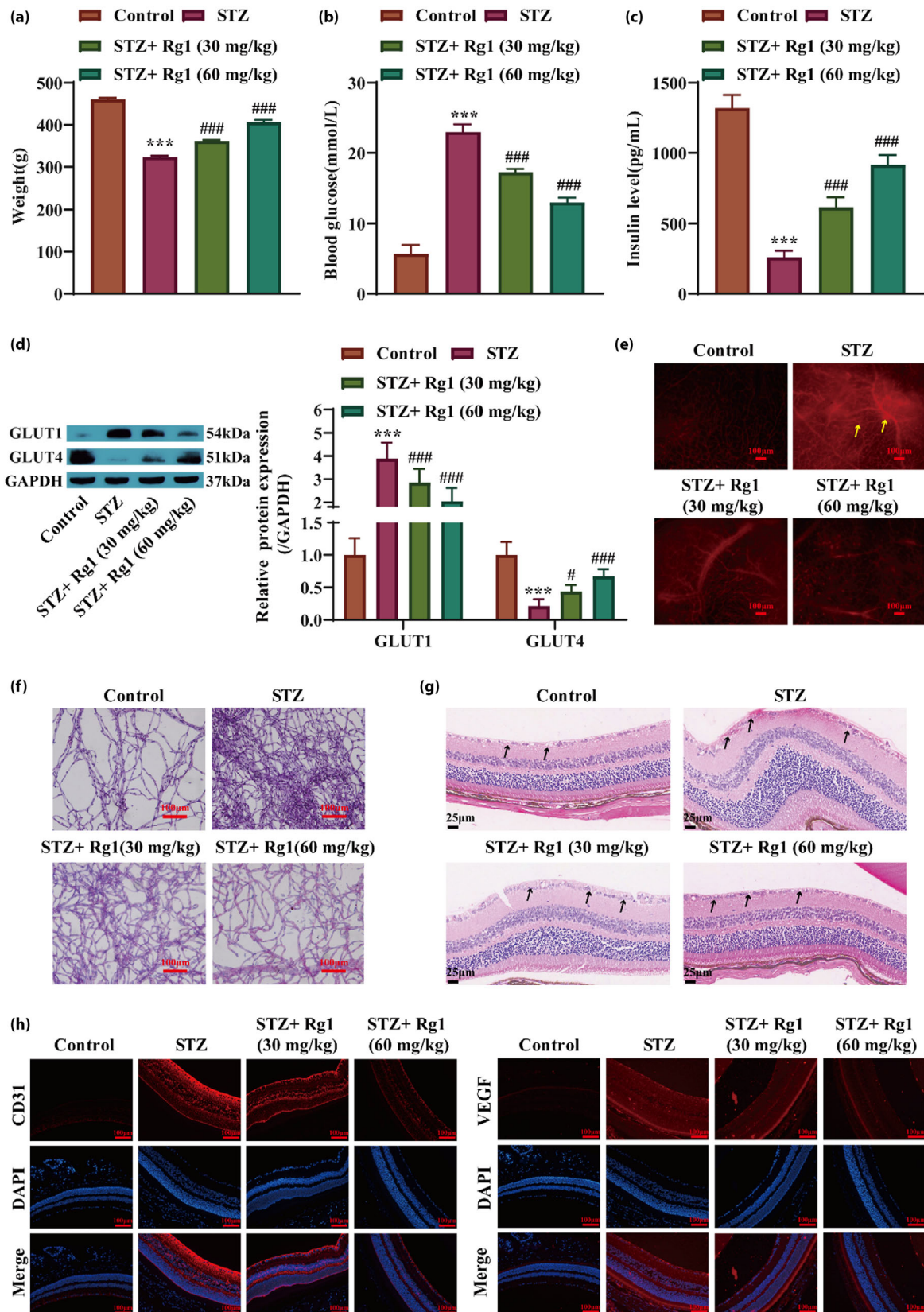


**Figure 1** | Ginsenoside Rg1 attenuates diabetes-induced retinal angiogenesis in vivo. (a) DR rats were administered ginsenoside Rg1 (30 or 60 mg/kg/day) by gavage, and the body weight of the rats was measured after 8 weeks; (b) DR rats were administered ginsenoside Rg1 (30 or 60 mg/kg/day) by gavage, and the fasting blood glucose level of the rats was measured after 8 weeks; (c) The serum insulin levels of rats were detected by ELISA; (d) Western blot was used to detect the expression of glucose transporters GLUT1 and GLUT4; (e) The rats were injected with Evans blue at the end of the experiment, and the permeability of retinal blood vessels was assessed by the Evans blue leakage test; (f) Retinal trypsin digestion was used to assess capillary degeneration; (g) HE staining was used to detect pathological changes in retinal tissue in the rats; (h) Immunofluorescence was used to detect the expression of CD31 and VEGF in rat retinal tissues. \*\*\* $P < 0.001$  vs Control; # $P < 0.05$ , ### $P < 0.001$  vs STZ ( $n = 5$ ).

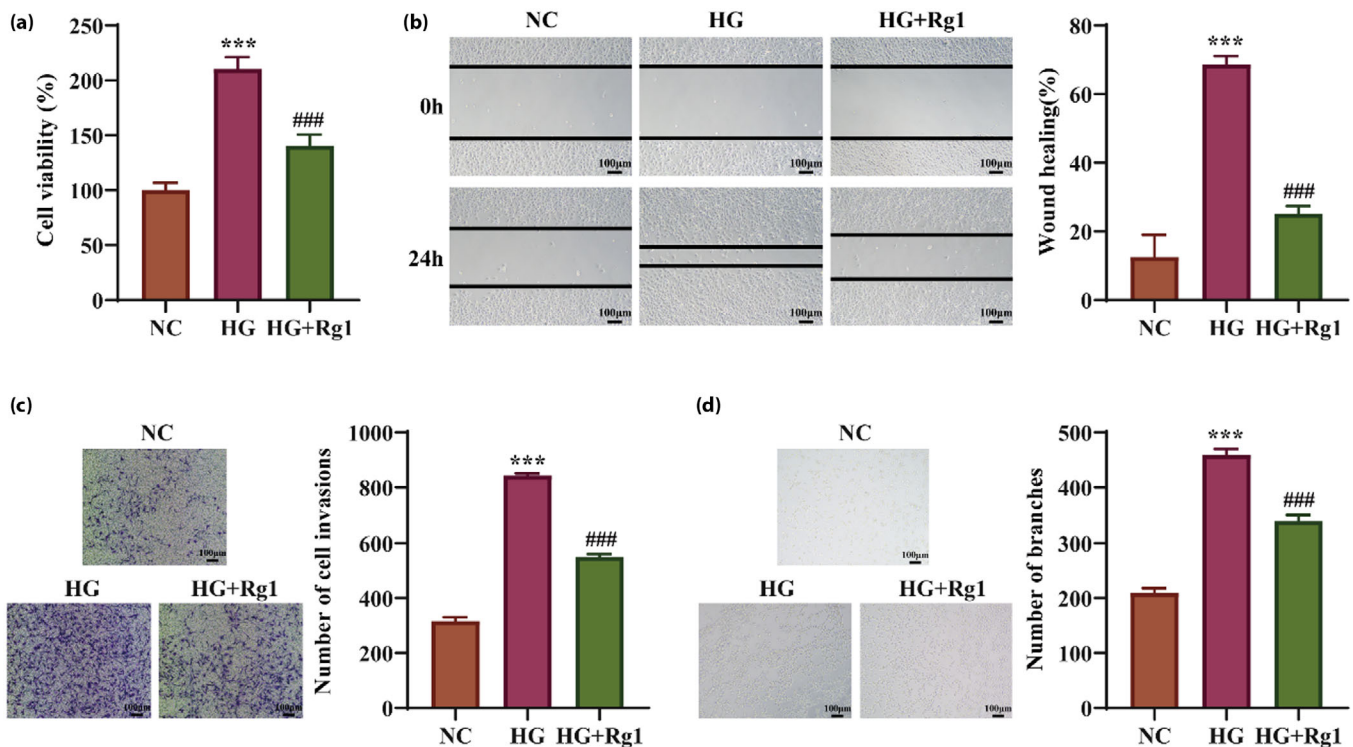


**Figure 2** | Ginsenoside Rg1 inhibits the high glucose-induced proliferation, migration, invasion, and angiogenesis of HRMECs. (a) HRMECs viability was detected by a CCK-8 assay; (b) HRMECs migration was detected by a scratch experiment; (c) HRMECs invasion was detected by a Transwell assay; (d) HRMECs angiogenesis was detected by a tube formation assay. \*\*\* $P < 0.001$  vs NC; ### $P < 0.001$  vs HG ( $n = 3$ ).

the cells, and the c-MYC protein degradation rate in the Rg1 group markedly increased compared with that in the NC group. These findings suggest that Rg1 has the potential to decrease the stability of the c-MYC protein (Figure 4d). Finally, we investigated the ubiquitination of c-MYC in HRMECs. The results indicated that Rg1 therapy enhanced the ubiquitination of c-MYC (Figure 4e). These findings suggest that by activating FBXW7, ginsenoside Rg1 may decrease the stability of the c-MYC protein.

#### Ginsenoside Rg1 inhibits c-MYC expression by downregulating miR-100-3p and targeting the activation of FBXW7

Previous studies have indicated that the control exerted by Rg1 on disease and angiogenesis primarily occurs via the

modulation of miRNA expression<sup>26–28</sup>. Therefore, we analyzed the differentially expressed miRNAs in DR through bioinformatics and found that 15 miRNAs were upregulated (miR-488, miR-577, and miR-100, among others) and that 14 miRNAs were downregulated (miR-150, miR-325, and miR-570, among others; Figure 5a). Three miRNAs (miR-488-5p, miR-577, and miR-100-3p) could bind to FBXW7 among the miRNAs with upregulated expression (Figure 5b). RT-qPCR analysis revealed that Rg1 suppressed the expression of miR-488-5p, miR-577, and miR-100-3p, with the most significant suppression observed for miR-100-3p (Figure 5c). As a result, miR-100-3p was chosen for further investigation. According to TargetScan prediction, a binding site exists between miR-100-3p and FBXW7 (Figure 5d). A dual-luciferase gene reporter assay confirmed that miR-100-3p can regulate FBXW7 expression



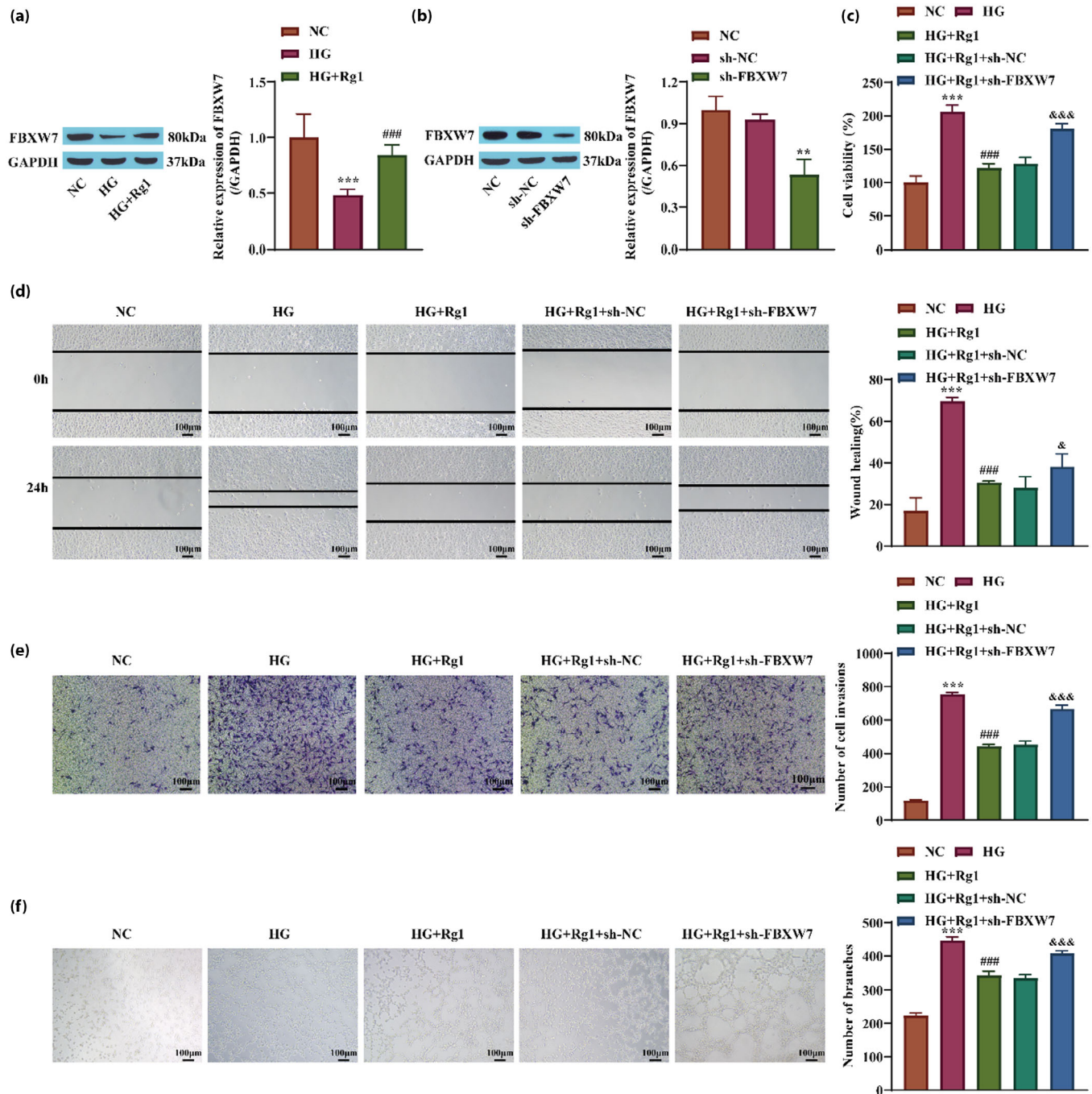


**Figure 3** | Ginsenoside Rg1 inhibits the high glucose-induced proliferation, migration, invasion, and angiogenesis of HRMECs by activating FBXW7. (a) Western blotting was used to detect the expression of FBXW7 in HRMECs; (b) Western blotting was used to detect the expression of FBXW7 in HRMECs to confirm the transfection efficiency of sh-FBXW7; (c) HRMECs viability was detected by a CCK-8 assay; (d) HRMECs migration was detected by a scratch experiment; (e) HRMECs invasion was detected by a Transwell assay; (f) A tube formation assay was performed to detect angiogenesis in HRMECs. \*\* $P < 0.01$ , \*\*\* $P < 0.001$  vs NC or sh-NC; ### $P < 0.001$  vs HG; & $P < 0.05$ , && $P < 0.001$  vs HG + Rg1 + sh-NC ( $n = 3$ ).

(Figure 5e). The levels of miR-100-3p in rat retinal samples were subsequently assessed. The results revealed that STZ triggered an increase in the miR-100-3p level, whereas treatment

with Rg1 led to the suppression of miR-100-3p expression (Figure 5B). The transfection efficiency of the miR-100-3p mimic was subsequently detected in HRMECs to confirm the



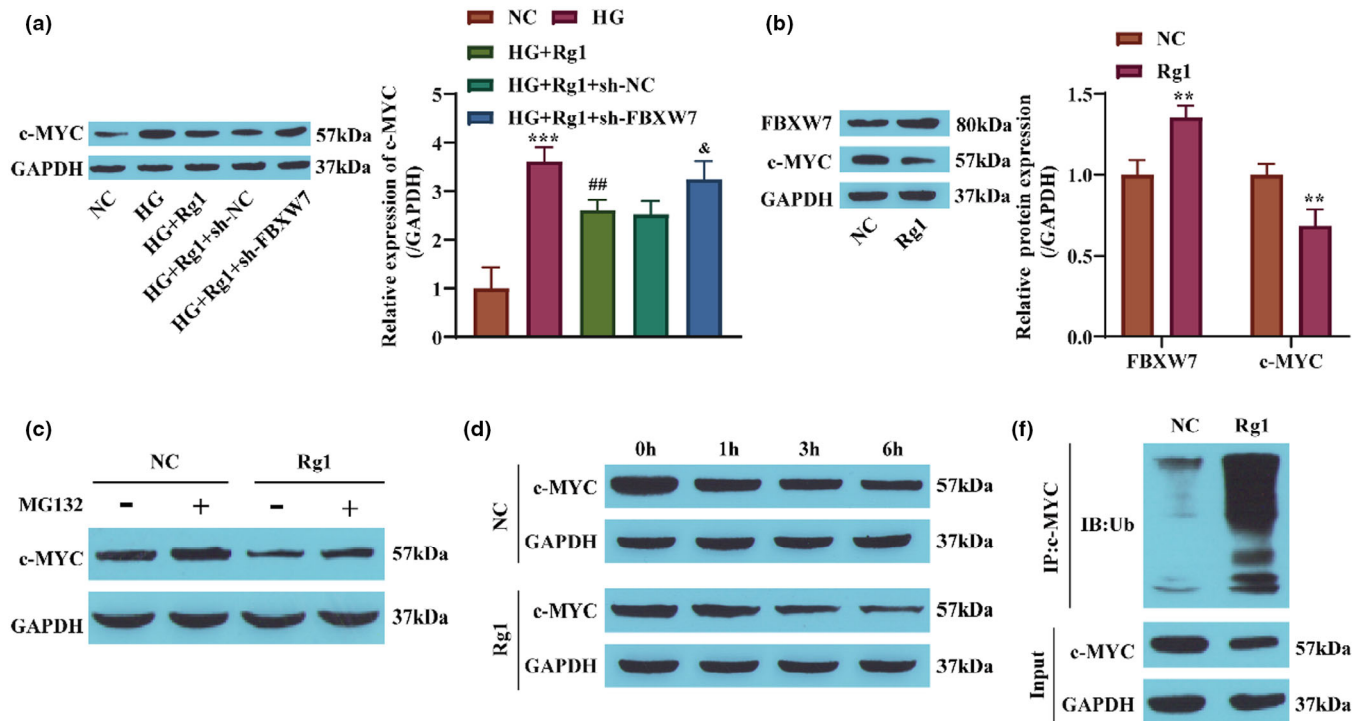


**Figure 4** | Ginsenoside Rg1-mediated activation of FBXW7 decreases the protein stability of c-MYC. (a) The expression of c-MYC in HRMECs was detected by Western blot; (b) Western blot detection of FBXW7 and c-MYC expression in HRMECs; (c) Western blot detection of c-MYC expression in cells treated with MG132 (proteasome inhibitor, 20  $\mu$ M); (d) Western blot analysis of c-MYC expression in cells treated with CHX (protein synthesis inhibitor, 100  $\mu$ g/mL); (e) Detection of the ubiquitination level of c-MYC. \*\* $P$  < 0.01, \*\*\* $P$  < 0.001 vs NC; ## $P$  < 0.01 vs HG; &#x2192; $P$  < 0.05 vs HG + Rg1 + sh-NC ( $n$  = 3).

success of the transfection (Figure 5f). The Western blot results also revealed that transfection of the miR-100-3p mimic inhibited the expression of FBXW7 and promoted the expression of c-MYC (Figure 5g). Finally, the inhibition of miR-100-3p and c-MYC expression by Rg1 and the promotion of FBXW7 expression were also partially reversed by miR-100-3p mimic treatment (Figure 5h,i). These findings suggest that ginsenoside Rg1 may inhibit c-MYC expression by targeting FBXW7 activation through the downregulation of miR-100-3p.

#### Overexpression of miR-100-3p attenuates the inhibitory effect of ginsenoside Rg1 on high glucose-induced HRMEC angiogenesis

Finally, the role of miR-100-3p in angiogenesis induced by elevated glucose levels in HRMECs was investigated. Compared with that in the HG group, the viability of HRMECs was notably lower following supplementation with Rg1. Conversely, the upregulation of miR-100-3p noticeably increased the viability of HRMECs (Figure 6a). In addition, the inhibitory effect of Rg1 treatment on the invasion and migration of HRMECs was reversed by the overexpression of miR-100-3p (Figure 6b,c). Rg1 treatment also inhibited the angiogenesis of HRMECs, and further overexpression of miR-100-3 promoted the angiogenesis

of HRMECs (Figure 6d). These findings suggest that ginsenoside Rg1 effectively attenuated HG-induced HRMEC angiogenesis by targeting miR-100-3p.

#### Rg1 alleviates the progression of DR in rats by inhibiting miR-100-3p

We further verified the effect of Rg1 on the progression of DR by regulating the expression of miR-100-3p in *in vivo* experiments. First, the results of body weight and blood glucose level detection in rats showed that Rg1 treatment could effectively increase the body weight and decrease the blood glucose level of rats, and the treatment with miR-100-3p mimic reversed the effect of Rg1 to a certain extent (Figure 7a,b). In addition, Rg1 treatment could increase the insulin level and the expression of glucose transporter GLUT4 and inhibit the expression of glucose transporter GLUT1; the treatment with miR-100-3p mimic also reversed the effect of Rg1 (Figure 7c,d). The results of Evans Blue leakage experiment showed that compared with the Control group, STZ treatment led to leakage of retinal blood vessels, Rg1 treatment could reduce the leakage of retinal blood vessels, but the treatment with miR-100-3p mimic weakened the effect of Rg1 (Figure 7e). The results of retinal trypsin digestion experiment and HE staining showed that the

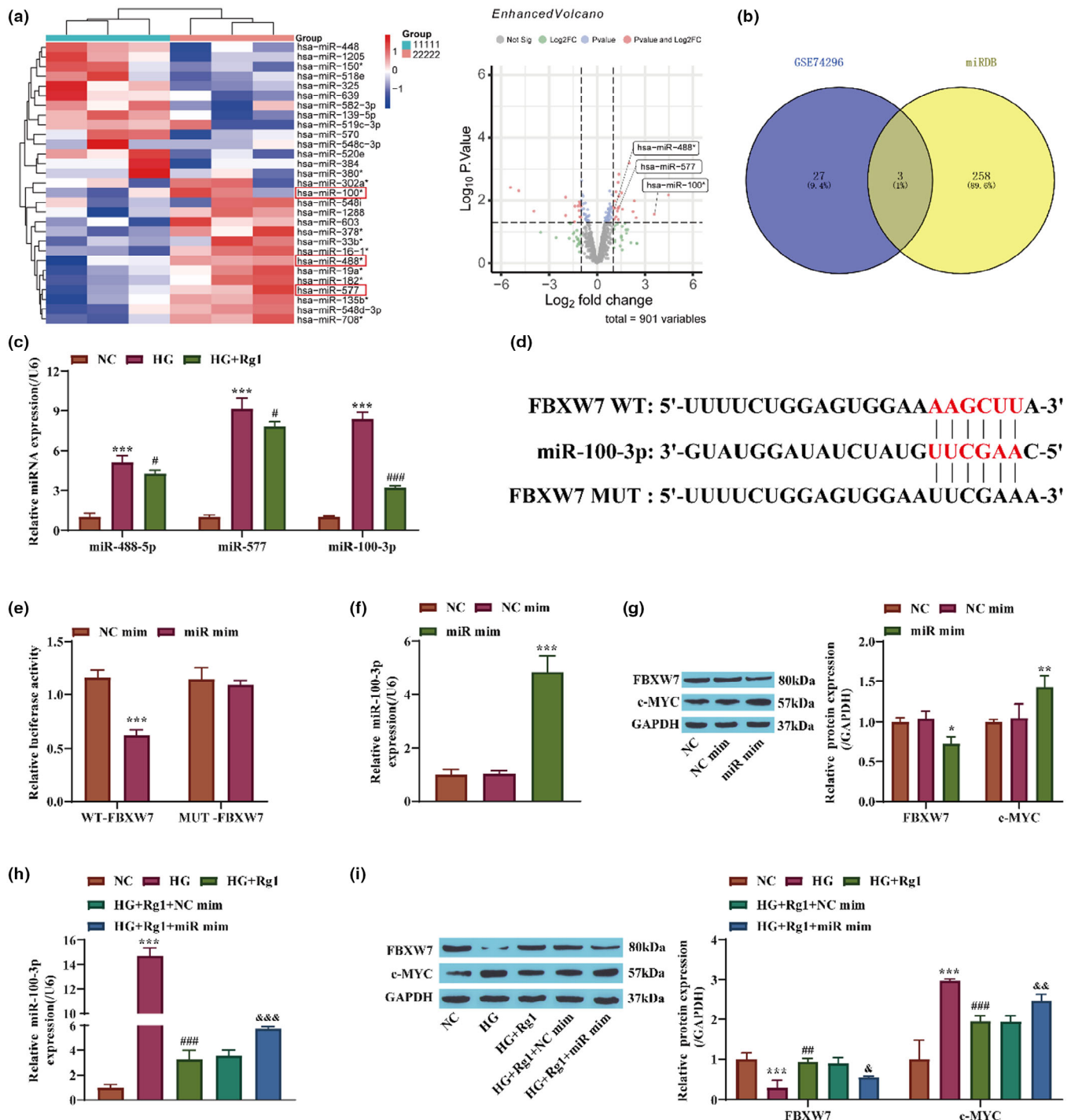


**Figure 5** | Ginsenoside Rg1 inhibits c-MYC expression through the downregulation of miR-100-3p and targeted activation of FBXW7. (a) Bioinformatics analysis data set of the GSE74296 differentially expressed miRNAs; (b) Bioinformatics analysis of the intersection of miRNAs that bind to FBXW7; (c) RT-qPCR was used to detect the expression of miR-488-5p, miR-577, and miR-100-3p in HRMECs; (d) The binding sequence between miR-100-3p and FBXW7 as predicted by TargetScan; (e) Dual-luciferase gene reporter analysis verified the relationship between miR-100-3p and FBXW7; (f) Transfection efficiency of the miR-100-3p mimic was detected by RT-qPCR; (g) The expression of FBXW7 and c-MYC was detected by Western blotting; (h) The expression of miR-100-3p was detected by RT-qPCR; (i) The expression of FBXW7 and c-MYC was detected by Western blotting. \* $P < 0.05$ , \*\* $P < 0.01$ , \*\*\* $P < 0.001$  vs NC or NC mimic; # $P < 0.05$ , ## $P < 0.01$ , ### $P < 0.001$  vs HG; & $P < 0.05$ , && $P < 0.01$ , &&& $P < 0.001$  vs HG + Rg1+ NC mim ( $n = 3$ ).

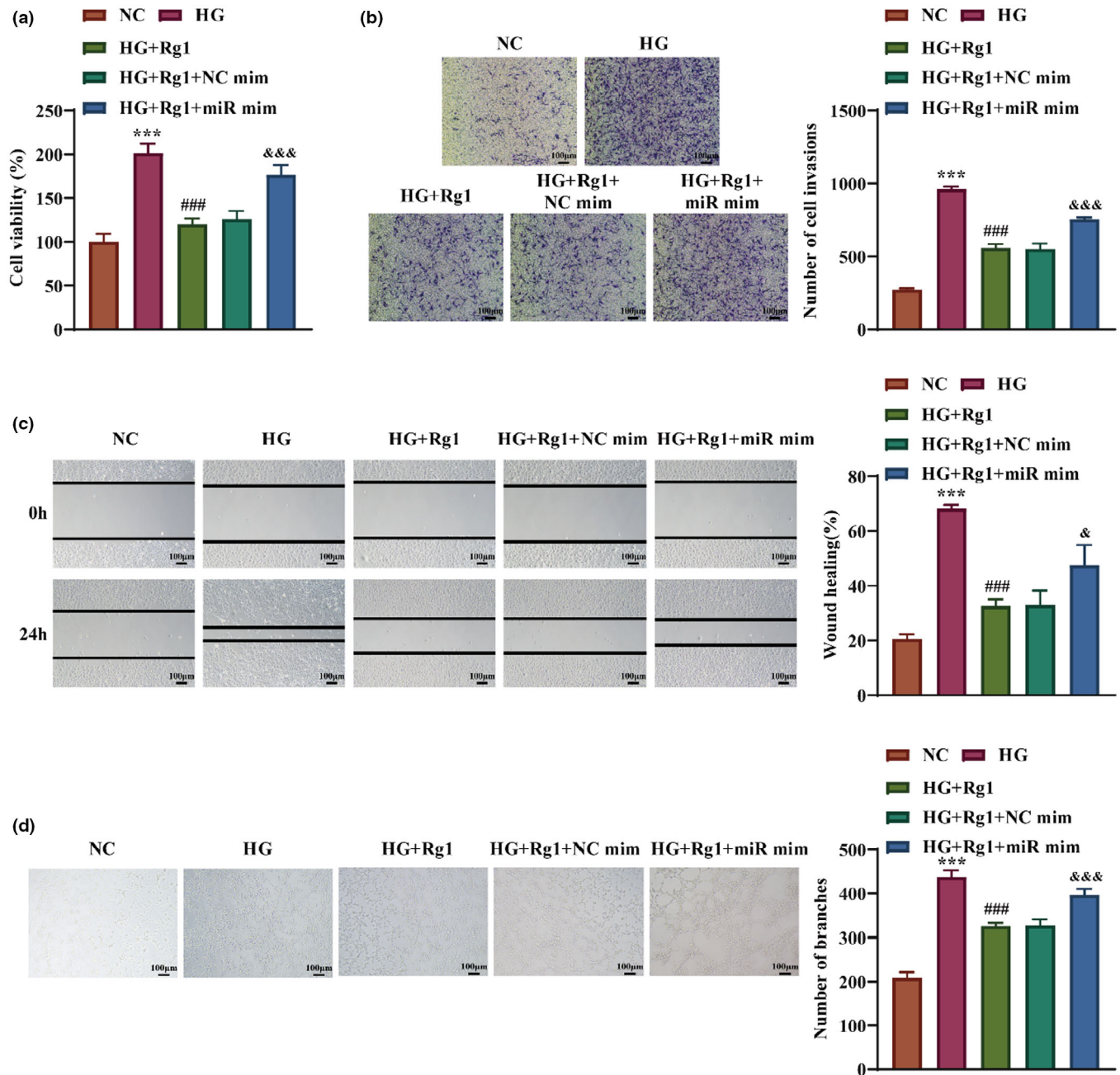


**Figure 6** | Overexpression of miR-100-3p attenuates the inhibitory effect of ginsenoside Rg1 on high glucose-induced HRMEC angiogenesis. (a) HRMECs viability was detected by a CCK-8 assay; (b) HRMECs invasion was detected by a Transwell assay; (c) HRMECs migration was detected by a scratch assay; (d) HRMECs angiogenesis was detected by a tube formation assay. \*\*\* $P < 0.001$  vs NC; ### $P < 0.001$  vs HG; & $P < 0.05$ , &&& $P < 0.001$  vs HG + Rg1+ NC mim ( $n = 3$ ).

improvement effect of Rg1 on capillary degeneration and retinal tissue lesions was reversed by the treatment with miR-100-3p mimic (Figure 7f,g). The results of immunofluorescence detection showed that the inhibitory effect of Rg1 on the expression of CD31 and VEGF was reversed to a certain extent by miR-

100-3p mimic (Figure 7h). Finally, the results of Western blot detection showed that compared with the Control group, the expression of FBXW7 was downregulated and the expression of c-MYC was upregulated in the STZ group. Rg1 treatment reversed the expression of FBXW7 and c-MYC, whereas the



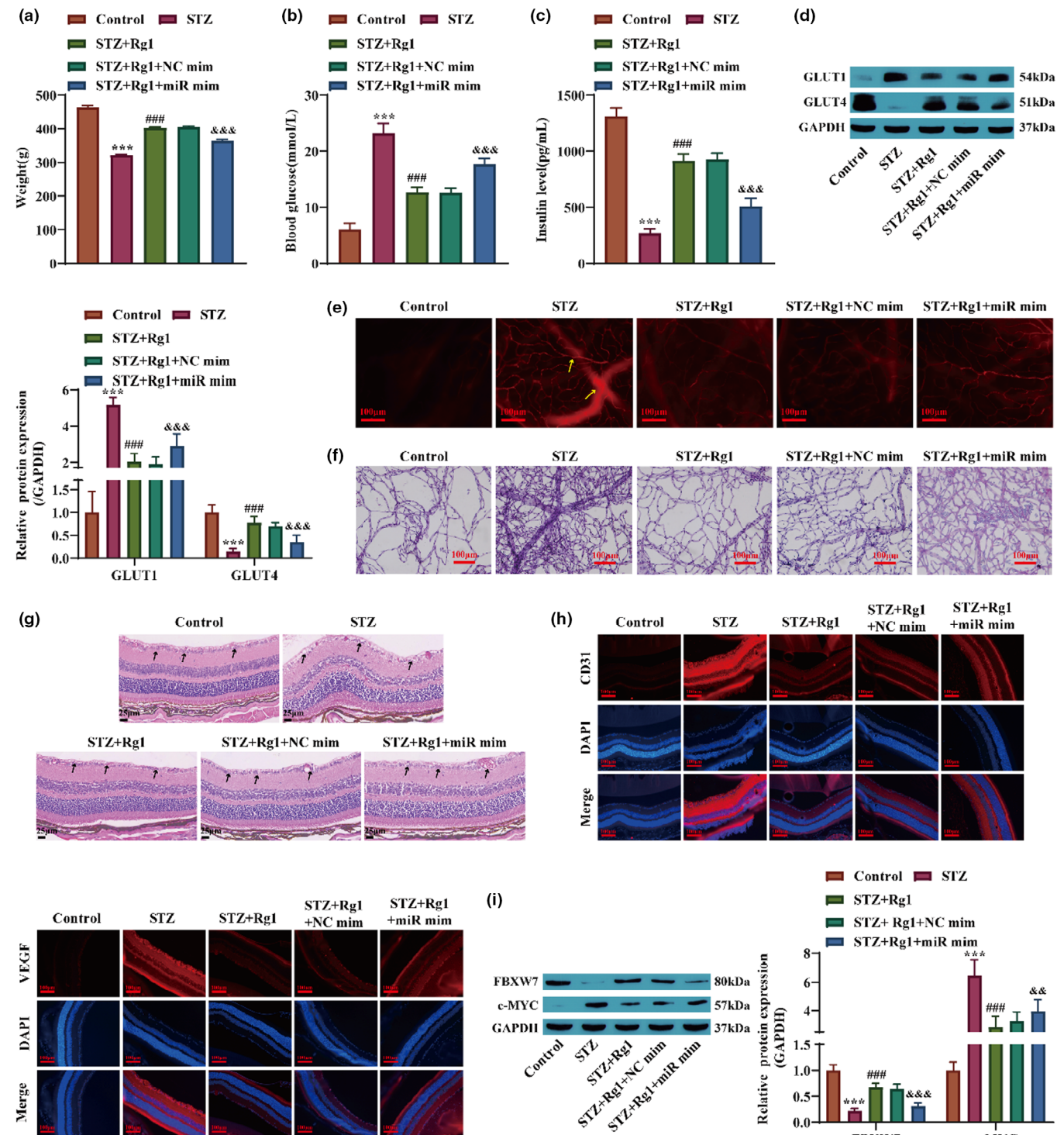


**Figure 7** | Rg1 alleviates the progression of DR in rats by inhibiting miR-100-3p. (a) Detection of rat body weight; (b) Detection of fasting blood glucose level in rats; (c) The serum insulin levels of rats were detected by ELISA; (d) Western blot was used to detect the expression of glucose transporters GLUT1 and GLUT4; (e) EvansBlue leak assay to evaluate retinal permeability in rats; (f) Retinal trypsinization assay to evaluate retinal capillary degeneration in rats; (g) HE staining was used to detect the pathological changes of rat retinal tissue; (h) Immunofluorescence detection of CD31 and VEGF expression in rat retinal tissue; (i) Western blot was used to detect the expression of FBXW7 and c-MYC. \*\*\* $P < 0.001$  vs Control; ### $P < 0.001$  vs STZ; &&& $P < 0.01$ , &&& $P < 0.001$  vs STZ + Rg1 + NC mim ( $n = 5$ ).

treatment with miR-100-3p mimic inhibited the effect of Rg1 again (Figure 7i). The above results indicate that Rg1 alleviates the progression of DR by inhibiting miR-100-3p in animals.

## DISCUSSION

DR is a visual impairment that can arise from diabetes. Over time, high levels of blood sugar in individuals with diabetes can harm small blood vessels in the eye, particularly microvessels found in the retina<sup>29</sup>. This harm can result in leakage of blood vessels, bleeding, and the formation of new blood vessels in the eye, which subsequently impacts the typical operation of the eye and may result in loss of vision in extreme situations<sup>30</sup>. Therefore, it is imperative to understand the development of DR and discover efficient drugs for treatments. Ginsenoside Rg1 is one of the main components of ginseng and has an antidiabetic effect<sup>31</sup>. In a previous study, Xue *et al.*<sup>32</sup> reported that Rg1 could inhibit HG-induced mesenchymal activation and fibrosis in proliferative DR. Barroso *et al.*<sup>33</sup> demonstrated that Rg1 can prevent hyperphosphorylated tau-induced synaptic nerve degeneration in retinal ganglion cells in the early stages of DR. Previous research has indicated that Rg1 holds promise as a drug for treating DR. Our study revealed that Rg1 not only inhibited HG-induced HRMEC proliferation, migration, invasion, and angiogenesis *in vitro* but also reduced vascular leakage and capillary degeneration and alleviated retinal dysfunction in STZ-induced models *in vivo*. This study is the first to demonstrate that Rg1 inhibits diabetes-induced retinal angiogenesis.

Recent studies have shown that the overexpression of FBXW7, an E3 ubiquitin ligase, reduces cell proliferation, migration, and lumen formation in oral squamous cell carcinoma<sup>34</sup>. Furthermore, it has the potential to control high glucose-triggered HRMEC proliferation, DNA synthesis, cell migration, and angiogenesis<sup>35</sup>. Therefore, we examined the expression levels of FBXW7 and observed a reduction in its expression in both DR rats and HRMECs induced by HG. Moreover, Hu *et al.*<sup>36</sup> reported that FBXW7 was underexpressed in DR mice and that overexpression of FBXW7 inhibited retinal angiogenesis in DR mice and inhibited HG-induced proliferation, migration, and angiogenesis of mouse retinal microvascular endothelial cells. This report is consistent with our findings, except that FBXW7 overexpression in our study was induced by Rg1 treatment. Notably, our study alongside that of Hu *et al.*<sup>36</sup> highlights similar outcomes in distinct mice and cells, supporting the importance of FBXW7 in DR treatment.

FBXW7, which serves as the principal ubiquitin ligase for c-MYC, can facilitate the ubiquitin-mediated breakdown of c-MYC and subsequently decrease its cellular expression<sup>37</sup>. The nuclear oncoprotein c-MYC plays multiple roles in cell proliferation, apoptosis, and transformation<sup>38</sup>. Moreover, Yao *et al.*<sup>39</sup> reported that downregulation of c-MYC inhibited endothelial cell proliferation, migration, and angiogenesis in oxygen-induced retinopathy. Therefore, we explored the relationships among Rg1, FBXW7, and c-MYC and found that

Rg1 can reduce the stability of c-MYC by activating FBXW7 and promoting its ubiquitination-mediated degradation, thereby inhibiting the proliferation, migration, invasion, and angiogenesis of HG-induced HRMECs. In previous studies, Daga *et al.*<sup>40</sup> reported that the inhibition of c-MYC led to decreased migration and proliferation in cisplatin-resistant bladder cancer cells. Sun *et al.*<sup>41</sup> demonstrated that the upregulation of c-MYC enhances the growth and mobility of tongue squamous cell carcinoma cells. Similarly, elevated levels of c-MYC can stimulate the formation of new blood vessels in renal cell carcinoma<sup>42</sup>. These findings indirectly support the promoting effects of c-MYC on HRMEC proliferation, migration, invasion, and angiogenesis observed in our study.

Additionally, a growing collection of evidence suggests that the regulatory impact of Rg1 on diseases and angiogenesis primarily occurs via the modulation of miRNA expression<sup>43,44</sup>. Moreover, miRNAs are key players in the progression of DR<sup>45</sup>. For example, a study by Gao *et al.*<sup>46</sup> demonstrated that increased levels of miR-34a-5p can enhance HG-induced endothelial-mesenchymal transition (EMT) and angiogenesis in HRMECs. Thus, our investigation focused on identifying abnormally upregulated miRNAs in DR, leading to the discovery that miR-100-3p is the most highly expressed miRNA that interacts with FBXW7. Importantly, Barros *et al.*<sup>47</sup> reported that miR-100-3p could worsen metabolic disorders caused by obesity, leading to disrupted glucose balance. Furthermore, Tashiro *et al.*<sup>17</sup> reported that miR-100-3p also plays a role in controlling the proliferation, migration, blood vessel growth, and lymphatic vessel growth of lymphatic endothelial cells. Building upon previous research findings as well as our own data, we examined how miR-100-3p functions in DR. We found that Rg1 inhibited the expression of miR-100-3p and that the overexpression of miR-100-3p promoted the expression of c-MYC by inhibiting FBXW7, thereby attenuating the inhibitory effect of Rg1 on HG-induced angiogenesis in HRMECs. This study presents a novel discovery that Rg1 impedes the progression of DR in rats by disrupting the actions of miR-100-3p, potentially alleviating blood vessel growth during DR development.

At present, this study has revealed the downstream mechanism of Rg1's influence on the expression of miR-100-3p, but it is still unclear how Rg1 regulates the expression of miR-100-3p. Based on the fact that miR-100-3p is an important regulator of Rg1's effect on DR, we hypothesized the potential regulatory mechanism of Rg1 on the expression of miR-100-3p. One possible mechanism is through transcriptional regulation. Rg1 has been shown to regulate the activity of the NF- $\kappa$ B transcription factor<sup>48</sup>. Transcription factors play an important role in the regulation of gene expression, so Rg1 may mediate the expression of miR-100-3p by affecting the transcriptional activity of specific transcription factors. Another possible mechanism is through epigenetic regulation. DNA methylation and histone modification in epigenetic modifications are also important regulators of gene expression. Rg1 has been shown to regulate Smad7 expression through epigenetically<sup>27</sup>. Therefore, Rg1 may

affect the epigenetic state of the miR-100-3p locus to regulate the expression of miR-100-3p. The above is only our conjecture based on the literature, and the detailed molecular mechanism of Rg1 regulating miR-100-3p needs to be further studied in the future.

In summary, our findings indicate that Rg1 can activate FBXW7 by inhibiting miR-100-3p, which leads to the ubiquitination and degradation of c-MYC. This process inhibits the proliferation, migration, invasion, and angiogenesis of HRMECs, thus slowing the progression of DR. Rg1 has the potential as a therapeutic agent for treating DR. However, our research has several limitations. First, we have not yet explored the upstream mechanism responsible for the upregulation of miR-100-3p expression in DR, a topic that could be studied from the perspective of circular RNA in the future. Second, we have not validated the function of the miR-100-3p/FBXW7/c-MYC axis in animal models, necessitating further experimental confirmation. Third, there is a need to investigate additional mechanisms involved in the development of DR, such as inflammation. Finally, our observations are based solely on cell and animal experiments and lack clinical trial verification. Therefore, further in-depth studies on the application of Rg1 for DR treatment are needed.

## ACKNOWLEDGMENTS

Not applicable.

## FUNDING

The study was supported by the Famous Doctor in Yunling [YNWR-MY-2020-088], and the Special Grant for High-level Personnel of Yunnan Province [L-2019020].

## DISCLOSURE

The authors declare no conflict of interest.

Approval of the research protocol: N/A.

Informed consent: N/A.

Approval date of registry and the registration no. of the study/trial: N/A.

Animal studies: All animal experiments complied with the ARRIVE guidelines and were performed in accordance with the National Research Council's Guide for the Care and Use of Laboratory Animals. All animal experimental protocols were approved by the Medical Ethics Committee of the Affiliated Hospital of Yunnan University (No. YNUCARE20210039).

## DATA AVAILABILITY STATEMENT

The data sets used and/or analyzed during the current study are available from the corresponding author upon reasonable request.

## REFERENCES

- Lin KY, Hsieh WH, Lin YB, *et al.* Update in the epidemiology, risk factors, screening, and treatment of diabetic retinopathy. *J Diabetes Investig* 2021; 12: 1322–1325.
- Zheng Y, He M, Congdon N. The worldwide epidemic of diabetic retinopathy. *Indian J Ophthalmol* 2012; 60: 428–431.
- Lois N, McCarter RV, O'Neill C, *et al.* Endothelial progenitor cells in diabetic retinopathy. *Front Endocrinol* 2014; 5: 44.
- Lechner J, O'Leary OE, Stitt AW. The pathology associated with diabetic retinopathy. *Vis Res* 2017; 139: 7–14.
- Liu Y, Wu N. Progress of nanotechnology in diabetic retinopathy treatment. *Int J Nanomedicine* 2021; 16: 1391–1403.
- Wang ZY, Liu JG, Li H, *et al.* Pharmacological effects of active components of Chinese herbal medicine in the treatment of Alzheimer's disease: A review. *Am J Chin Med* 2016; 44: 1525–1541.
- Liu H, Wang J, Liu M, *et al.* Antiobesity effects of ginsenoside Rg1 on 3T3-L1 preadipocytes and high fat diet-induced obese mice mediated by AMPK. *Nutrients* 2018; 10: 830.
- Chu Y, Zhang W, Kanimozhi G, *et al.* Ginsenoside Rg1 induces apoptotic cell death in triple-negative breast cancer cell lines and prevents carcinogen-induced breast tumorigenesis in Sprague Dawley rats. *Evid Based Complement Alternat Med* 2020; 2020: 8886955.
- Bao S, Zou Y, Wang B, *et al.* Ginsenoside Rg1 improves lipopolysaccharide-induced acute lung injury by inhibiting inflammatory responses and modulating infiltration of M2 macrophages. *Int Immunopharmacol* 2015; 28: 429–434.
- Zhang L, Zhu M, Li M, *et al.* Ginsenoside Rg1 attenuates adjuvant-induced arthritis in rats via modulation of PPAR- $\gamma$ /NF- $\kappa$ B signal pathway. *Oncotarget* 2017; 8: 55384–55393.
- Bi S, Ma X, Wang Y, *et al.* Protective effect of ginsenoside Rg1 on oxidative damage induced by hydrogen peroxide in chicken splenic lymphocytes. *Oxid Med Cell Longev* 2019; 2019: 8465030.
- Yu H, Zhen J, Yang Y, *et al.* Ginsenoside Rg1 ameliorates diabetic cardiomyopathy by inhibiting endoplasmic reticulum stress-induced apoptosis in a streptozotocin-induced diabetes rat model. *J Cell Mol Med* 2016; 20: 623–631.
- Xue L, Hu M, Li J, *et al.* Ginsenoside Rg1 inhibits high glucose-induced proliferation, migration, and angiogenesis in retinal endothelial cells by regulating the lncRNA SNHG7/miR-2116-5p/SIRT3 Axis. *J Oncol* 2022; 2022: 6184631.
- Tiwari D, Peariso K, Gross C. MicroRNA-induced silencing in epilepsy: Opportunities and challenges for clinical application. *Dev Dyn* 2018; 247: 94–110.
- Zhao X, Ling F, Zhang GW, *et al.* The correlation between MicroRNAs and diabetic retinopathy. *Front Immunol* 2022; 13: 941982.
- Polus A, Bociaga-Jasik M, Czech U, *et al.* The human immunodeficiency virus (HIV1) protease inhibitor saquinavir activates autophagy and removes lipids deposited in lipid droplets. *J Physiol Pharmacol* 2017; 68: 283–293.
- Tashiro K, Yoshioka Y, Ochiya T. Extracellular vesicles from adipose-derived stem cells relieve extremity lymphedema in mouse models. *Plast Reconstr Surg* 2023; 152: 1011–1021.



18. Shao J, Fan G, Yin X, *et al.* A novel transthyretin/STAT4/miR-223-3p/FBXW7 signaling pathway affects neovascularization in diabetic retinopathy. *Mol Cell Endocrinol* 2019; 498: 110541.
19. Zhang G, Zhu Q, Fu G, *et al.* TRIP13 promotes the cell proliferation, migration and invasion of glioblastoma through the FBXW7/c-MYC axis. *Br J Cancer* 2019; 121: 1069–1078.
20. Chang HC, Hsieh TH, Lee YW, *et al.* c-Myc and viral cofactor Kaposin B co-operate to elicit angiogenesis through modulating miRNome traits of endothelial cells. *BMC Syst Biol* 2016; 10: 1.
21. Zhang J, Chen C, Wu L, *et al.* C-myc contributes to the release of Müller cells-derived proinflammatory cytokines by regulating lncRNA MIAT/XNIP pathway. *Int J Biochem Cell Biol* 2019; 114: 105574.
22. Kumari S, Kamboj A, Wanjar M, *et al.* Nephroprotective effect of Vanillic acid in STZ-induced diabetic rats. *J Diabetes Metab Disord* 2021; 20: 571–582.
23. Tian M, Yang J, Yan X, *et al.* Knockdown of lncRNA TUG1 alleviates diabetic retinal vascular dysfunction through regulating miR-524-5p/FGFR2. *Bioengineered* 2022; 13: 12661–12672.
24. Gu Y, Hu D, Xin Y, *et al.* Transthyretin affects the proliferation and migration of human retinal microvascular endothelial cells in hyperglycemia via hnRNPA2B1. *Biochem Biophys Res Commun* 2021; 557: 280–287.
25. Gu Q, Wei HF. PLAG1 promotes high glucose-induced angiogenesis and migration of retinal endothelial cells by regulating the Wnt/ $\beta$ -catenin Signalling pathway. *Folia Biol Praha* 2022; 68: 25–32.
26. Zhai K, Duan H, Wang W, *et al.* Ginsenoside Rg1 ameliorates blood-brain barrier disruption and traumatic brain injury via attenuating macrophages derived exosomes miR-21 release. *Acta Pharm Sin B* 2021; 11: 3493–3507.
27. Zhang R, Li X, Gao Y, *et al.* Ginsenoside Rg1 epigenetically modulates Smad7 expression in liver fibrosis via MicroRNA-152. *J Ginseng Res* 2023; 47: 534–542.
28. Chan LS, Yue PY, Mak NK, *et al.* Role of microRNA-214 in ginsenoside-Rg1-induced angiogenesis. *Eur J Pharm Sci* 2009; 38: 370–377.
29. Toh H, Smolentsev A, Bozadjian RV, *et al.* Vascular changes in diabetic retinopathy—a longitudinal study in the Nile rat. *Lab Invest* 2019; 99: 1547–1560.
30. Liu K, Gao X, Hu C, *et al.* Capsaicin ameliorates diabetic retinopathy by inhibiting poldip2-induced oxidative stress. *Redox Biol* 2022; 56: 102460.
31. Liu Q, Zhang FG, Zhang WS, *et al.* Ginsenoside Rg1 inhibits glucagon-induced hepatic gluconeogenesis through Akt-FoxO1 interaction. *Theranostics* 2017; 7: 4001–4012.
32. Xue LP, Fu XL, Hu M, *et al.* Rg1 inhibits high glucose-induced mesenchymal activation and fibrosis via regulating miR-2113/RP11-982M15.8/Zeb1 pathway. *Biochem Biophys Res Commun* 2018; 501: 827–832.
33. Ying Y, Zhang YL, Ma CJ, *et al.* Neuroprotective effects of ginsenoside Rg1 against hyperphosphorylated tau-induced diabetic retinal neurodegeneration via activation of IRS-1/Akt/GSK3 $\beta$  signaling. *J Agric Food Chem* 2019; 67: 8348–8360.
34. Li C, Lin XF, Wang JN, *et al.* FBXW7 inhibited cell proliferation and invasion regulated by miR-27a through PI3K/AKT signaling pathway and epithelial-to-mesenchymal transition in oral squamous cell carcinoma. *Eur Rev Med Pharmacol Sci* 2020; 24: 3701–3709.
35. Tian Y, Ye L, Shao J, *et al.* The interface targeting hnRNPA2B1 regulates the repression of transthyretin against human retinal microvascular endothelial cells in high-glucose environment. *Diabet Med* 2023; 40: e15125.
36. Hu L, Lv X, Li D, *et al.* The anti-angiogenesis role of FBXW7 in diabetic retinopathy by facilitating the ubiquitination degradation of c-Myc to orchestrate the HDAC2. *J Cell Mol Med* 2021; 25: 2190–2202.
37. Mihashi Y, Mizoguchi M, Takamatsu Y, *et al.* C-MYC and its Main ubiquitin ligase, FBXW7, influence cell proliferation and prognosis in adult T-cell leukemia/lymphoma. *Am J Surg Pathol* 2017; 41: 1139–1149.
38. Guan L, Zou Q, Liu Q, *et al.* HSP90 inhibitor Ganetespib (STA-9090) inhibits tumor growth in c-Myc-dependent esophageal squamous cell carcinoma. *Onco Targets Ther* 2020; 13: 2997–3011.
39. Yao X, Xue Y, Ma Q, *et al.* 221S-1a inhibits endothelial proliferation in pathological angiogenesis through ERK/c-Myc signaling. *Eur J Pharmacol* 2023; 952: 175805.
40. Daga M, Pizzimenti S, Dianzani C, *et al.* Ailanthone inhibits cell growth and migration of cisplatin resistant bladder cancer cells through down-regulation of Nrf2, YAP, and c-Myc expression. *Phytomedicine* 2019; 56: 156–164.
41. Sun J, Lu Z, Deng Y, *et al.* Up-regulation of INSR/IGF1R by C-myc promotes TSCC tumorigenesis and metastasis through the NF- $\kappa$ B pathway. *Biochim Biophys Acta Mol basis Dis* 2018; 1864(5 Pt A): 1873–1882.
42. Park JY, Kim PJ, Shin SJ, *et al.* FGFR1 is associated with c-MYC and proangiogenic molecules in metastatic renal cell carcinoma under anti-angiogenic therapy. *Histopathology* 2020; 76: 838–851.
43. Chen P, Li X, Yu X, *et al.* Ginsenoside Rg1 suppresses non-small-cell lung cancer via MicroRNA-126-PI3K-AKT-mTOR pathway. *Evid Based Complement Alternat Med* 2022; 2022: 1244836.
44. Kwok HH, Chan LS, Poon PY, *et al.* Ginsenoside-Rg1 induces angiogenesis by the inverse regulation of MET tyrosine kinase receptor expression through miR-23a. *Toxicol Appl Pharmacol* 2015; 287: 276–283.
45. Sadashiv, Sharma P, Dwivedi S, *et al.* Micro (mi) RNA and diabetic retinopathy. *Indian J Clin Biochem* 2022; 37: 267–274.
46. Cao X, Xue LD, Di Y, *et al.* MSC-derived exosomal lncRNA SNHG7 suppresses endothelial-mesenchymal transition and

- tube formation in diabetic retinopathy via miR-34a-5p/XBP1 axis. *Life Sci* 2021; 272: 119232.
47. Barroso A, Santos-Marcos JA, Perdices-Lopez C, *et al.* Neonatal exposure to androgens dynamically alters gut microbiota architecture. *J Endocrinol* 2020; 247: 69–85.
48. Luo M, Yan D, Sun Q, *et al.* Ginsenoside Rg1 attenuates cardiomyocyte apoptosis and inflammation via the TLR4/NF- $\kappa$ B/NLRP3 pathway. *J Cell Biochem* 2020; 121: 2994–3004.

## SUPPORTING INFORMATION

Additional supporting information may be found online in the Supporting Information section at the end of the article.

**Figure S1.** Ginsenoside Rg1 regulates the expression of FBXW7, c-MYC, and miR-100-3p. (a) Western blot analysis of the expression of FBXW7 and c-MYC in rat retinal tissues; (b) RT-qPCR analysis of miR-100-3p expression in rat retinal tissues. \*\*\* $P < 0.001$  vs Control; \*\* $P < 0.01$ , ### $P < 0.001$  vs STZ ( $n = 5$ ).